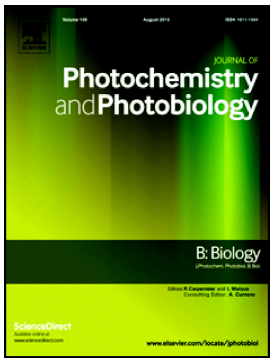

Altered lipid acyl chain length controls energy dissipation in light-harvesting complex II proteoliposomes by hydrophobic mismatch

Dan-Hong Li, Sam Wilson, Giulia Mastroianni, Alexander V. Ruban

PII: S1011-1344(23)00112-4

DOI: https://doi.org/10.1016/j.jphotobiol.2023.112758

Reference: JPB 112758

To appear in: *Journal of Photochemistry & Photobiology, B: Biology*

Received date: 28 April 2023

Revised date: 18 July 2023

Accepted date: 19 July 2023

Please cite this article as: D.-H. Li, S. Wilson, G. Mastroianni, et al., Altered lipid acyl chain length controls energy dissipation in light-harvesting complex II proteoliposomes by hydrophobic mismatch, *Journal of Photochemistry & Photobiology, B: Biology* (2023), https://doi.org/10.1016/j.jphotobiol.2023.112758

Altered lipid acyl chain length controls energy dissipation in light-harvesting complex II proteoliposomes by hydrophobic mismatch

Dan-Hong Li[a], Sam Wilson[a], Giulia Mastroianni[a], Alexander V. Ruban[a*]

[a] Department of Biochemistry, School of Biological and Behavioural Sciences, Queen Mary University of London, London, E1 4NS, United Kingdom

D.-H. Li: danhong.li@qmul.ac.uk;
S. Wilson: btx276@qmul.ac.uk;
G. Mastroianni: g.mastroianni@qmul.ac.uk;

*Corresponding authors: a.ruban@qmul.ac.uk

Abstract

In plants, the major light-harvesting antenna complex (LHCII) is vital for both light harvesting and photoprotection in photosystem II. Previously, we proposed that the thylakoid membrane itself could switch LHCII into the photoprotective state, qE, via a process known as hydrophobic mismatch. The decrease in the membrane thickness that followed the formation of ΔpH was a key fact that prompted this idea. To test this, we made proteoliposomes from lipids with altered acyl chain length (ACL). Here, we show that ACL regulates the average chlorophyll fluorescence lifetime of LHCII. For liposomes made of lipids with an ACL of 18 carbons the lifetime was ~2 ns, like that for the thylakoid membrane. Furthermore, LHCII appears to be quenched in proteoliposomes with an ACL both shorter and longer than 18 carbons. The proteoliposomes made of short ACL lipids display structural heterogeneity revealing two quenched conformations of LHCII, each having characteristic 77 K fluorescence spectra. One conformation spectrally resembles isolated LHCII aggregates, whilst the other resembles LHCII immobilized in polyacrylamide gels. Overall, the decrease in the ACL appears to produce quenched conformations of LHCII, which renders plausible the idea that the trigger of qE is the hydrophobic mismatch.

Keywords: acyl chain length, fluorescence quenching, hydrophobic mismatch, LHCII, proteoliposomes, protein/lipid interaction

1. Introduction

The photosynthetic membrane is a well-organized assembly composed of a variety of proteins and lipids. One major constituent, the major light-harvesting complex (LHCII) is highly concentrated with chlorophylls (Chl) and carotenoids (Car) and is the main supplier of excitation energy to photosystem II (PSII) reaction centers. Whilst this process remains efficient under low-to-moderate light, under intense light, the photosynthetic efficiency of PSII can be dramatically impeded in a process referred to as photoinhibition [1,2]. To regulate light harvesting, LHCII can shift between light-harvesting and energy-dissipative conformations, thereby safely dispersing the excess absorbed energy as heat, in a process known as non-photochemical quenching (NPQ). Its major component forms and relaxes on a timescale of seconds to minutes and is known as qE [3]. It has been demonstrated that the minimum requirement for qE is a sufficient pH gradient (ΔpH) and trimeric LHCII [4,5]. *In vivo*, typically the hydrophobic zeaxanthin and the PSII subunit S (PsbS) protein are also required to fine-tune the qE process allowing it to be triggered at more moderate levels of ΔpH [6-8].

To understand the mechanism of this triggering process, phenomena associated with the qE mechanism must be explored in the membrane environment. Firstly, LHCII aggregation was proposed as to be part of the mechanism of qE [4,9]. Electron microscopy on negatively-stained grana membranes [10] and freeze-fracture electron microscopy provided evidence that aggregation of LHCII particles in the membrane indeed takes place in the qE state *in vivo*, and is promoted by zeaxanthin [11]. Secondly, LHCII mobility was strongly decreased in the qE state, with PsbS acting to increase membrane fluidity in the transitions between light and dark [12,13]. Moreover, molecular dynamics simulations indicated that the way PsbS increases membrane fluidity could be through blocking interactions between the thylakoid lipid digalactosyl diglyceride (DGDG) and the LHCII complex [14]. Thirdly, the light-induced thinning of the thylakoid membrane was observed and initially thought to be related to the formation of the ΔpH gradient [15,16]. Later, thin section electron microscopy revealed that the membrane thinning correlated with qE, rather than ΔpH [12]. Lastly, the flattening of the LHCII complex in the vertical plane was suggested [17] as well as the twisting of neoxanthin in the qE state [18,19]. Furthermore, qE was associated with conformational change in LHCII even in systems where aggregation was either unlikely or impossible. This was shown through analysis of the quenching using cross-linkers [20], high hydrostatic pressure [21], polymerization in polyacrylamide gels [22], and single-molecule fluorescence spectroscopy [23].

Whilst each of the above points has been relatively well characterized in relation to qE, the open question on whether the ΔpH or the concomitant light-induced membrane thinning is directly the trigger of LHCII's transition into the quenched state is still not settled yet. However, we recently proposed that the membrane thinning associated with qE could act globally to sort LHCII into quenching

microdomains, in a process known as hydrophobic mismatch [24]. The process is known to cause conformational change and aggregation of membrane proteins [25,26]. In essence, any exposure of hydrophobic moieties of proteins or lipids to water causes the increase in free energy of a membrane, thus membrane proteins with equivalent hydrophobic areas are driven together and effectively sorted in the membrane [25,27]. Therefore, we proposed the hypothesis that membrane thinning (the case of positive mismatch) or flattening of LHCII (negative mismatch) could reasonably provide the drive for LHCII aggregation and conformational change, and finally provide the driving force for qE.

To test this hypothesis, we have constructed LHCII in proteoliposomes. Here, we focus on a minimal system to disentangle the effects of the membrane system on LHCII, independent of the PsbS protein, zeaxanthin, and ΔpH, according to the recent report that clearly demonstrated the minimum requirement of qE *in vivo* was ΔpH and trimeric LHCII [5]. The LHCII proteoliposomes consist of phosphatidylcholine (PC) lipids with varying acyl chain lengths (ACL). As the ACL is directly related to membrane thickness [28,29], this system can act as an *in vitro* model to test the applicability of the hydrophobic mismatch hypothesis to the NPQ mechanism. PC is a bilayer-forming lipid, forms vesicles, and has defined structures in solution, and is thus a model for many proteoliposomal studies [30-34]. By altering the ACL of the lipid, we have obtained artificial membranes with varying thicknesses. As the natural thylakoid membrane is composed of lipids with a majority ACL of 18 carbons [35,36], possessing a 2 ns fluorescence lifetime *in vivo* [37,38], we used the 18 carbon ACL PC (DOPC, hereafter 18PC) as a control, to create a simpler system than that of natural thylakoid lipids. To avoid oversaturation of LHCII-LHCII interactions, we made our liposomes with a Chl-to-Lipid molar ratio of 1:70. Hereafter, we utilized the chain lengths 10PC, 14PC, 18PC, and 24PC to simulate different membrane thickness, relative to the LHCII complex itself.

2. Materials and methods

2.1 Plant material and LHCII preparation

Major LHCII complexes were isolated from Spinach (*Spinacia oleracea*), which were obtained from a local market and dark-adapted for 45 minutes prior to any experiment. Stacked thylakoid membranes and PSII-enriched BBY particles were isolated from dark leaves as described previously [39,40], using a ratio of 0.6% (w/v) n-dodecyl-β-D-maltoside (β-DDM) in 1 mg Chl mL^{-1} to solubilize proteins. For protein isolation, a concentration of 400–600 µg Chl was loaded on a sucrose density gradient and centrifuged for 18–20 h at 40,000 rpm at 4°C [41]. Chl was quantified as described previously [42]. Isolated LHCII proteins were desalted in a PD-10 desalting column (Cytiva, UK) in a buffer containing 20 mM HEPES (pH 7.6), 10 mM NaCl, and 0.03% (w/v) β-DDM.

2.2 Proteoliposomal preparation

Phosphatidylcholine (PC) in chloroform (Avanti Polar Lipids, USA) was used for the liposome preparation. The saturated PC 1,2-didecanoyl-*sn*-glycero-3-phosphocholine (10:0 PC), and unsaturated PC 1,2-dimyristelaidoyl-*sn*-glycero-3-phosphocholine (14:1 (*Δ*9-cis) PC), 1,2-dioleoyl-*sn*-glycero-3-phosphocholine (18:1 (*Δ*9-cis) PC), and 1,2-dinervonoyl-*sn*-glycero-3-phosphocholine (24:1 (cis) PC) were each used. Proteoliposomes were prepared as previously described [34], with more details as follows. 1 mg PC in chloroform was placed in a 5 mL glass vial with the solvent dried under nitrogen gas. The thin film was resuspended in 1 mL buffer containing 20 mM HEPES (pH 7.6) and 10 mM NaCl with the final lipid concentration of 1 mg mL^{-1}. This solution was shaken thoroughly with a vortex mixer for 2 min and subsequently passed 11 times through a 100 nm pore extruder (Avanti Polar Lipids, USA) to form the liposome. 0.03% (w/v) *β*-DDM was added to the liposome and incubated on ice for 15 min. Then, the LHCII proteins were added to the liposome mixture and sonicated in a water bath for 5 min. To remove detergent from the liposomes, 90 mg mL^{-1} BioBeads SM-2 resin (Bio-Rad, USA) was added and incubated for 4 h at 4°C. BioBeads were then removed through one layer of muslin cloth, followed by centrifugation at 15,000 rpm for 15 min at 4°C to pellet any LHCII aggregates that were not incorporated into proteoliposomes. An initial Chl-to-Lipid ratio of 1:70 (mol/mol) was used. Samples were further purified by adding 1 mL of the proteoliposomal preparation onto sucrose density gradients (10, 20, 30, 45% sucrose (w/v)) and centrifuged at 40,000 rpm 4°C for 17–18 h. Hereafter, the layer of proteoliposomes was extracted and stored at 4 °C for up to 12 h until measurement.

2.3 Calculation of protein surface occupancy in the LHCII proteoliposomes

The number of lipid molecules per liposome (N_L) can be calculated through the use of the equation [43], as

$$N_L = \frac{4\pi}{A_L}\left(\frac{d}{2}\right)^2 + \frac{4\pi}{A_L}\left[\frac{d}{2} - h\right]^2 \qquad (1)$$

where A_L represents the size of each lipid molecule in the plain of the liposome, here taken as 0.35 nm^2, as calculated previously for PC lipids [44]. d is the liposomal diameter taken from the DLS measurements (Fig. 1), and h is the bilayer thickness taken from the cryo-EM measurements from 18PC (Fig. S2), and other membrane thicknesses with various ACL are calculated by 0.7 nm intervals for every four carbons according to the thickness of 18PC.

The number of trimeric LHCII protein complexes per proteoliposome (P) can further be calculated as

$$P = \frac{N_L}{R_{LC}}\left(\frac{1}{N_C}\right) \qquad (2)$$

where R_{LC} is the measured Lipid-to-Chl molar ratio of the proteoliposomal solution, and N_C is the number of Chls in a LHCII trimer, taken from the crystal structure (Protein Data Bank code: 1rwt) [45].

The percentage surface occupancy of LHCII in each proteoliposomal preparation ($P_{\%}$) can be further calculated as

$$P_{\%} = 10^2 \left[\frac{A_P P}{4\pi}\left(\frac{d}{2}\right)^{-2}\right] \qquad (3)$$

where A_P is the approximate effective area of LHCII in the lipid membrane, here taken as 30 nm^2, roughly approximated from the crystal structure [45] and freeze-fracture electron microscopy data [11].

2.4 Dynamic light scattering

Dynamic light scattering (DLS) measurements were performed with DynaPro (Protein Solutions, Wyatt). The laser light source was 824.7 nm and the detector was placed at the scattering angle of 90°. A 3 mm path-length quartz cell was filled with 45 µL sample solution. Before a cell was introduced into the instrument, its outer surfaces were wiped gently with a sheet of soft lens-cleaning tissue. Every measurement was set for a 2 min wait time to allow solutions to be at rest and to get rid of bubbles in the cell. Laser power was set at 20% intensity. At least 50 successive DLS measurements were performed per sample with 10 s acquisition time at 20°C. For each liposome condition, the measurements consisted of three biological sample replicates. The particle size is described and calculated in terms of hydrodynamic diameter d_H by the Stokes-Einstein equation ($d_H = kT/3\eta\pi D$), where k is the Boltzmann's constant, T is the absolute temperature, η is the viscosity of the solvent, and D is the diffusion coefficient [46]. The wider bin in the histogram after 200 nm in 24PC was limited by the technique, for the intensity-weighted size distribution was acquired from intensity fluctuations of the light scattered by particles. This is considered to give even greater weighting to the large particles so that the bin becomes wider along with the bigger particle size.

2.5 Cryo-electron microscopy

For the morphological observation, 4 µL proteoliposomal sample was adjusted to 0.5 mg mL^{-1} lipid and loaded onto glow-discharged lacey copper grids with ultrathin carbon film (400 mesh, EMR, UK). Samples were vitrified at –183°C in liquid ethane using a Leica automatic plunge freezer EM GP2 (Leica Microsystems, Germany) with a 2.6 s blot time under 80% relative humidity at 4°C. The frozen grids were imaged on a JEM-2100 plus electron microscope (JEOL, Japan) equipped with a OneView Gatan camera (Gatan, USA) using the SerialEM software package [47]. The analysis of cryo-EM images allows us to measure the nearest-neighbor distances with a spatial resolution of 0.22 nm (single-pixel size in XY

direction). The original magnification of the measurement was ×50,000. Images were analyzed using the Image J software [48]. Statistical significance between results was determined using a Student's *t*-test.

2.6 Room temperature (293 K) chlorophyll fluorescence lifetime measurement

Time-correlated single photon counting (TCSPC) measurements were performed using a FluoTime 200 ps fluorometer (PicoQuant, Germany). Fluorescence lifetime decay kinetics were measured on LHCII and proteoliposomes (6 μg Chl mL^{-1}) using excitation provided by a 470 nm laser diode at a 20 MHz repetition rate, with emission detected at 680 nm with a 2 nm slit width. These settings were chosen to be far below the onset of singlet-singlet exciton annihilation (< 0.1 pJ). The instrument response function (IRF) was ~50 ps. For lifetime analysis, FluoFit software (PicoQuant, Germany) was used by a multi-exponential model with iterative reconvolution of the IRF. The quality of the fits was judged by the χ^2 parameter. Average lifetimes were calculated from an amplitude-weighted lifetime as described previously [49]. All the measurements were taken at room temperature.

2.7 Steady-state absorption spectroscopy and fluorescence spectroscopy

Absorption measurements were performed on an Aminco DW-2000 UV/Vis spectrophotometer (Olis Inc., USA). Absorption spectra were measured between 350 nm and 750 nm with 1 nm increments.

Low-temperature (77 K) emission spectra were recorded by a FluoMax-3 spectrophotometer (HORIBA Jobin Yvon, France). The sample was cooled to 77 K with a liquid-nitrogen-cooled cryostat. Samples were measured at a concentration of 6 μg total Chl mL^{-1}. Samples were excited at 436 nm with a 5 nm spectral bandwidth. The emission spectra were acquired from 600 nm to 800 nm with a 1 nm slit and through a 630 nm long-pass filter. Fluorescence spectra were corrected in the program supplied by the manufacturer.

2.8 SDS-PAGE

The LHCII protein purity was confirmed by sodium dodecyl sulfate-polyacrylamide gel electrophoresis (SDS-PAGE) analysis. Proteins were added to the laemmli buffer and heated at 90°C for 10 min. 12% acrylamide/bis-acrylamide linear gels were employed (Mini-PROTEAN TGX Stain-Free Precast Gels, BioRad, USA). Gels were stained with Coomassie InstantBlue (Abcam, UK). An equal amount of Chl (0.33 μg) was loaded onto each lane per sample. The measurements were proceeded by three biological sample replicates.

3. Results

3.1 Structural and morphological features of the proteoliposomes

From dynamic light scattering (DLS) measurements, the hydrodynamic radii (R) of the LHCII proteoliposomes were obtained (Fig. 1). In general, particles in each condition were symmetrically distributed with a prominent peak, indicating that spherical liposomes were well formed, other than aggregates with random sizes. Fitting Gaussian curves to the histogram, it can be seen that unlike other proteoliposomes, the 10PC LHCII proteoliposome contains two main size distributions, with smaller particle sizes at 35 ± 2 nm (± SEM) and a broad peak at 101 ± 2 nm, likely indicating that the 10PC LHCII proteoliposome has a more complicated composition. Generally, proteoliposomes have a trend of increasing radius depending on longer acyl chain lengths (ACL), with the 24PC condition possessing a broad distribution and the biggest size at 173 ± 5 nm. Furthermore, as a control sample without protein incorporated, the size of empty 18PC liposomes was measured (Fig. S1), which had an average radius of 83 ± 2 nm, similar to the 18PC LHCII proteoliposomes with the representative sizes of 81 ± 1 nm (Fig. 1C). The 14PC possesses the average size in 67 ± 1 nm. We would like to further mention that both the free unincorporated LHCII aggregates and empty liposomes were not present in the preparations these measurements. This was ensured by the centrifugation step after the addition of BioBeads and further sucrose gradient separation steps (Fig. S4). Furthermore, the cryo-EM images for the proteoliposomal

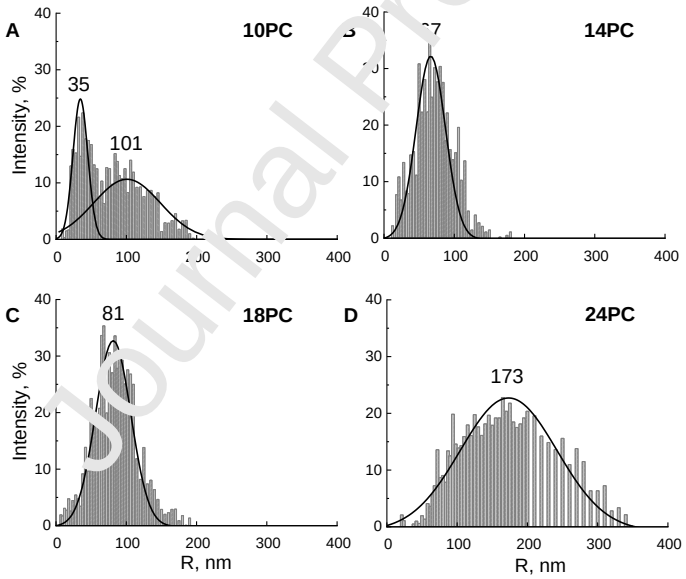

samples shown in Fig. S5 did not reveal any LHCII aggregates.

Fig. 1. **Size distributions for LHCII proteoliposomes with altered acyl chain length (ACL) determined by dynamic light scattering (DLS).** Hydrodynamic radius (R) displays with a range of ACL (n) on LHCII proteoliposomes, which were constructed by phosphatidylcholine (PC), named nPC. The molar ratio of chlorophyll-to-lipid was 1:70. The measurements were mean ± SEM of three replicates, with fitting lines proceeded by Gaussian fitting. The fitting related full width at half maximum (FWHM) were evaluated as 25 ± 1 nm (± SD) and 112 ± 9 nm for 10PC, 49 ± 2 nm for 14PC, 59 ± 2 nm for 18PC, and 162 ± 12 nm for 24PC.

As the *in vivo* thylakoid membrane lipids mostly possess an ACL of 18 [35,36,50], 18PC LHCII proteoliposomes offer a comparable condition. The cryo-EM images of the 18PC proteoliposomes are shown in Fig. S2A. The proteoliposomes are unilamellar and display a bilayer membrane thickness of 3.72 ± 0.02 nm (± SEM) (Fig. S2B) from the microscopic images. As a control, the image of the empty 18PC liposome without LHCII incorporated is shown in Fig. S3A. Without LHCII, the bilayer thickness of the membrane decreased by 0.2 nm (Fig. S3B), indicating that LHCII protein may also have a minor modulating effect on membrane thickness [51].

To have an idea of the physiological status of the LHCII in proteoliposomes, the Chl insertion ratios were calculated for each preparation (Fig. 2) [42]. The 18PC condition has the highest yield of 93.0% ± 2.0 (± SEM) of total Chl insertion, followed by a yield of 9[illegible]% ± 0.7 in 14PC. This likely indicates that the 18PC maintains a favorable environment for the LHCII complex. At 10PC, only 75.8% ± 2.3 of the starting Chl ended up in the proteoliposome, whilst the 24PC LHCII proteoliposome, only 57.7% ± 4.5 of total Chl was inserted into the membrane. Unlike the 14PC and 18PC which likely represent bilayer thicknesses close to *in vivo* dimensions of the thylakoid membrane, the Chl insertion ratios do highlight the 10PC and 24 PC conditions as physiological extremes.

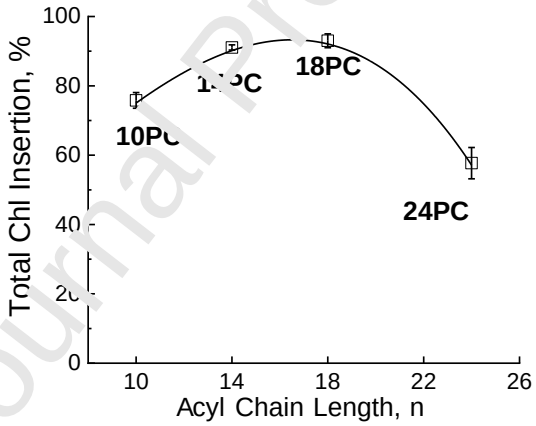

Fig. 2. **Chlorophyll (Chl) insertion ratio of LHCII proteoliposome with series of ACL at 293 K.** The Chl insertion ratios were measured by 80% acetone extraction [42], with which the Chl in the form of aggregates were removed through centrifugation. Data are the average of three independent experiments ± SEM. The difference in insertion ratios between 14PC and 18PC is not statistically significant (P > 0.05), which is determined via a Student's *t*-test.

Based on the structural findings mentioned earlier, we can estimate the percentage surface occupancy of LHCII ($P_{\%}$) for each type of proteoliposome, providing insights into the density of the LHCII complex on the liposome's surface. The average $P_{\%}$ for 18PC and 14PC is determined to be 4.79% and 4.80% respectively. In contrast, the 24PC condition exhibits a lower average $P_{\%}$ of 3.31%, potentially attributed to the combination of a lower insertion ratio and larger liposome sizes. Regarding the 10PC

condition, the data were segregated into two subsets based on the observed heterogeneity in each sample (Fig. 1A). The smaller 10PC liposomes display a $P_{\%}$ of 3.58%, while the larger 10PC liposomes exhibit a slightly higher $P_{\%}$ of 3.90%. Hence, despite variations in Chl insertion rates among the different liposome types, the $P_{\%}$ values remain consistently low and comparable for each condition. This suggests that the initial low Chl-to-Lipid ratio limits the chances of a significant degree of LHCII aggregation in all types of liposomes.

Considering that the alteration of the membrane thickness through ACL affects both the sizes and the Chl insertion in proteoliposome, it is likely that multiple numbers of LHCII trimers per proteoliposome could provide LHCII with the possibility of aggregation in the membrane [52]. Yet, small $P_{\%}$ values less than ~5% indicate a low LHCII occupancy in each proteoliposome condition. The $P_{\%}$ percentage roughly equates to an average of 23 LHCII trimers per 14PC proteoliposome, 33 LHCII trimers per 18PC proteoliposome, 104 LHCII trimers per 24PC proteoliposome, and at extreme 5 LHCII trimers in the smaller 10PC liposome and 42 LHCII trimers in the larger 10PC liposome. For example, despite $P_{\%}$ values of ~3.3% and ~3.6% for the 24PC and the smaller 10PC conditions, there are 104 and 5 LHCII complexes in each, respectively. 104 trimers seems to be more likely to self-associate and form large oligomers more readily than in conditions with only 5 trimers [52]. However, since the liposome size varies one must compare the protein densities in the liposomes instead. Therefore, the calculated densities of trimers for the 10PC, 14PC, 18PC and 24PC were 1.25, 1.60, 1.60 and 1.19 trimers per 1000 nm^2, respectively. This indicates that in 10PC and 24 PC liposomes with quenched chlorophyll fluorescence the concentration of LHCII was even lower than in the 'unquenched' liposomes with 18CP.

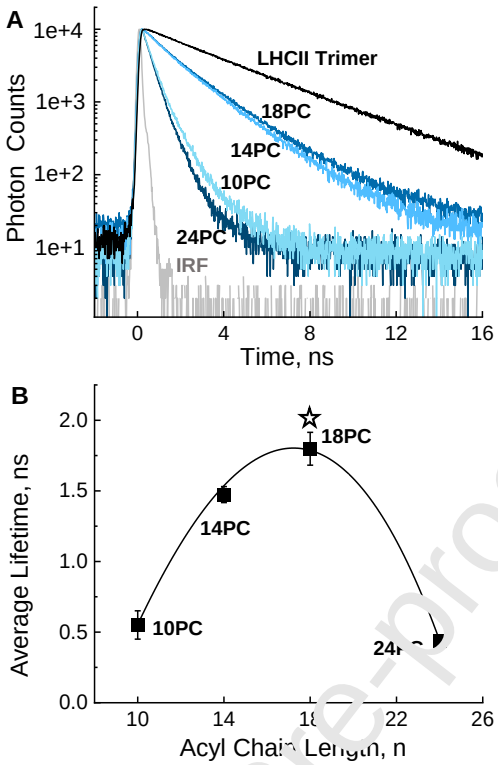

3.2 Biophysical characterization of the proteoliposomes

Fig. 3. **The correlation between average fluorescence lifetime and series of ACL for LHCII proteoliposome at room temperature.** *A*, 293 K fluorescence decay traces of trimeric LHCII in detergent and LHCII proteoliposomes. The excitation wavelength was at 470 nm, and the emission was measured at 680 nm. *B*, Correlation between the average amplitude-weighted fluorescence lifetimes (τ_{avg}) and ACL at 293 K. Line depicts the best fit of a 3-exponential mode for a lifetime. Data are means of three independent experiments ± SEM. There is no significant difference in lifetime comparing 10PC to 24PC ($P > 0.05$), which is determined via a Student's *t*-test. The 14PC shows a significant quenched lifetime compared to 18PC with a P value of 0.04 by the paired-*t*-test report. The open star corresponds to the 2 ns fluorescence lifetime of the natural thylakoid with a lipid ACL of 18. Statistical analyses of average lifetime are listed in **Supplementary Table 1**.

Through the measurement of the samples' fluorescence lifetimes, the extent of LHCII quenching can be quantified. The isolated trimeric LHCII complex shows an average fluorescence lifetime of 3.65 ns (Fig. 3) with a high purity identified by SDS-PAGE (Fig. S6), however, *in vivo*, while proteins preventing concentration quenching on Chls, LHCII is already partially quenched with a 2 ns Fm lifetime (when all PSII reaction centers are closed by light) [37,38]. For the 18PC LHCII proteoliposome (Fig. 3A), the sample has an average lifetime of 1.80 ± 0.12 ns (± SEM), similar to the Fm lifetime measured in thylakoid membranes [37,38]. In each condition, the average fluorescence lifetimes are 1.47 ± 0.06 ns for 14PC, 0.55 ± 0.10 ns for 10PC, and 0.44 ± 0.04 ns for the 24PC condition. Most strikingly, whilst the decrease in ACL from 18PC to 14PC does result in quenching of the complex, larger quenching has been seen in both the 10PC and 24PC conditions (Fig. 3B). It is likely that the membrane dimensions of both

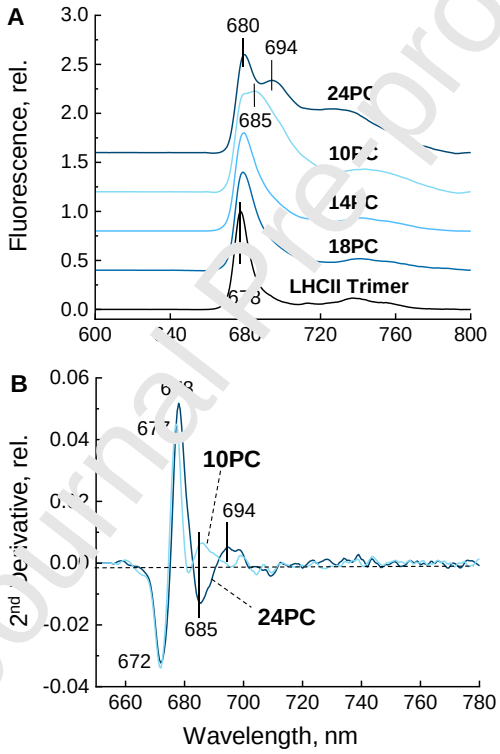

are causing a conformational change of LHCII into the quenched state.

Fig. 4. **Appearance of the 77 K fluorescence emission spectra and the inverted 2nd derivative spectra of the LHCII proteoliposomes.** *A*, 77 K fluorescence emission spectra of trimeric LHCII in detergent and nPC LHCII proteoliposomes with altered ACL (n). The excitation wavelength was 436 nm. Spectra are normalized to their respective F680 peak. Figures are set as larger offsets according to higher peak at ~694 band. *B*, 2nd derivative of the fluorescence spectra for 24PC and 10PC LHCII proteoliposomes.

To investigate this further, we recorded 77 K fluorescence emission spectra in each condition (Fig. 4A). As a reference, the LHCII trimer in detergent shows a single characteristic peak at 678 nm (F680)

and its associated vibronic satellite. LHCII in 18PC LHCII proteoliposome shows a broader F680 spectrum similar to that of *in vivo* thylakoid membrane at room temperature [37]. Following the decline of the ACL from 18PC, 14PC to 10PC, the shoulder peak at ~694 nm (F700) shows increasing contribution, causing the main F680 peak to be effectively broadened. Concurrently, the 678 nm band shows a gradual red shift of 2 nm to 680 nm, indicating a lower excited energy of the terminal emitter. For the 24PC condition, the F700 at 694 nm can be distinguished as an individual peak. However, the 10PC condition has a very different profile. Here, it appears that there is a large broadening of the 685 nm peak (F685), resembling a similar 77 K fluorescence spectra to that of LHCII immobilized in polyacrylamide gels [22]. A further contrast between the 10PC and 24PC can be seen through the 2nd derivative of the fluorescence spectra (Fig. 4B). Here, it is clear that there are opposite contributions in each condition to 685 nm and 694 nm. The positive peak at 685 nm in 10PC LHCII proteoliposome (light blue) elucidates a bulk of molecules responsible for the 685 nm broadened peak. However, this is not present in the 24PC condition (dark blue). Therefore, the 2nd derivative spectra are strong evidence supporting the idea that LHCII has a distinctly different protein conformation in 10PC compared to 24PC, where the chlorophyll environment was apparently different. However, the average chlorophyll fluorescence lifetimes for LHCII in 10PC and 24PC are very similar.

In the structural characterization of the proteoliposomes, the 10PC particles show unique bimodal distributions in sizes, as illustrated by DLS. To separate these two forms of proteoliposome in 10PC, further sucrose gradient purification was performed (Fig. 5A). Here, we managed to resolve two bands, hereafter, band 1 (B1) and band 2 (B2). Through measurement of the fluorescence lifetimes at room temperature (Fig. 5B), 10 PC proteoliposomes in B1 were calculated with an average lifetime of 0.75 ns, whilst B2 has a shorter average lifetime of 0.29 ns. Thus, indicating that the denser proteoliposomes in B2 are more quenched. Concomitantly, the 77 K fluorescence emission spectra are also highly divergent (Fig. 5C). B1 has a broad shoulder at ~683 nm, resembling the bulk 10PC condition as in Fig. 4A. However, B2 is quite similar to the spectrum of the 24PC condition. Here, a dominant F700 band can be seen alongside the F680. The sorting of LHCII into two distinct conformations here is likely reflective of the changes in structural morphology, and of the overall strain on the LHCII complex enforced by the 10PC membrane.

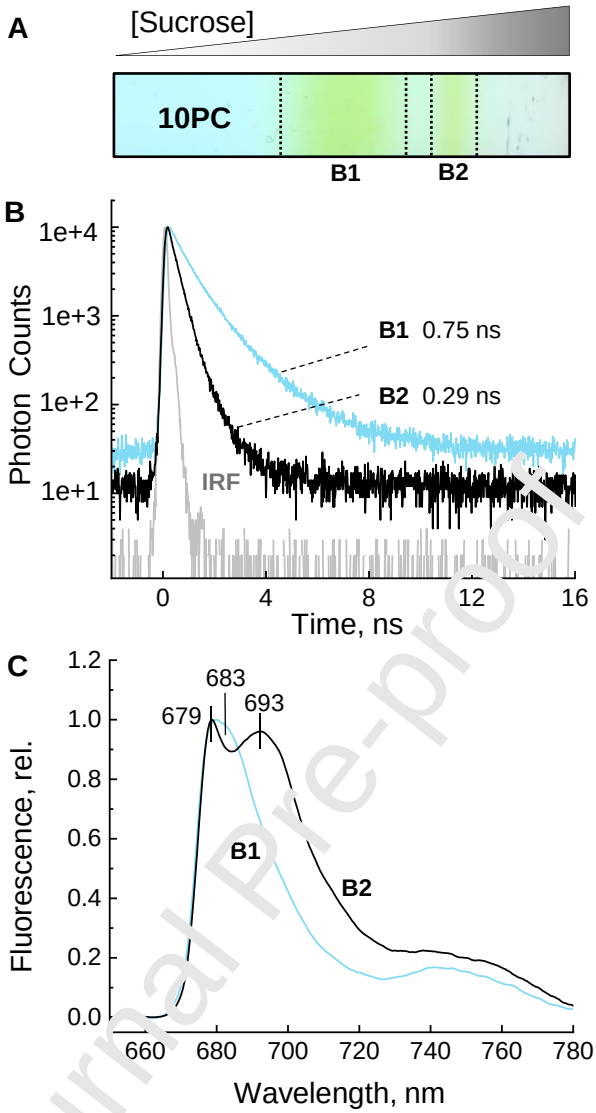

Fig. 5. **Bi-phasic distributions of 10PC LHCII proteoliposome and fluorescence properties.** *A*, Sucrose density gradient separates the two-bands distributions (B1, B2) of 10PC LHCII proteoliposome at room temperature. *B*, 293 K lifetime distributions of B1 (blue trace) and B2 (black trace). The excitation wavelength was 470 nm and probed at 680 nm. *C*, 77 K fluorescence emission spectra of B1 and B2 when excited at 436 nm.

4. Discussion

In the thylakoid membrane, the dynamics of the membrane and the lipids therein play intimate roles in fine-tuning the organization and conformation of the protein complexes within. Whilst many *in vitro* works have focussed on the role that individual lipid types play [35,52-54], the role of the apparent thylakoid membrane thinning has remained largely elusive [12]. Here, we have constructed a range of LHCII proteoliposomes from lipids with altered ACL to simulate thylakoid membrane thinning processes.

4.1 The role of lipid acyl chain length in determining the structural features of proteoliposomes

As a large amount of imaging research has been done on liposomes, the strong evidence to show that the membrane thickness is determined by the ACL [28,29,31,32,55]. As previously reported, the typical membrane thickness of 18 ACL was 3.6–3.7 nm [28,34], and the membrane bilayer thickness decreases by approximately 0.6–0.7 nm for every four carbons [28,29,56]. Therefore, the most straightforward strategy is relating the membrane thickness to the ACL of lipids.

However, the 10PC condition displays a certain morphological diversity. Here, there is a bimodal distribution of both liposomal size and particle density, representing two fluorescence quenching extents. 10PC likely represents a condition wherein LHCII experiences structural stress, as further highlighted by a reduced yield of chlorophyll insertion into the liposome. On one hand, it is more likely that the extremely short 10 carbons of ACL in lipids can trigger the shrinking of LHCII into conformational change, thus allowing LHCII could conform to comfortably reside within. On the other hand, the bi-phasic distributions may be linked with a change in the phase transition temperature (Tm) from the fluid liquid crystalline state to the ordered gel state of lipids [31,32]. The Tm has been shown to be heavily dependent on the ACL of the liposome with various protein concentrations [55,57-59]. Thus, it is possible that the Tm of our 10PC condition is around the temperature of the measurements, therefore, there will be a heterogeneous population of proteoliposomes in both the gel phase and fluid liquid phase, which may explain the biphasic distribution of 10PC seen here

4.2 The relationship between membrane thickness and energy-dissipative states of LHCII

Here, we have made liposomes at a moderate LHCII density, similar to previously published works on both liposomes [52,60,61] and nanodiscs [62-66]. The 18PC condition shows an average fluorescence lifetime and spectra similar to that of LHCII in native thylakoid membranes [37,38]. Whilst it has been well characterized that increasing LHCII density in proteoliposomes causes quenching [34,52,67], here we show that any deviations in membrane thickness from that of dark-adapted *in vivo* membranes also cause LHCII to convert into a quenched conformation [11]. It is interesting that the light-harvesting states of LHCII are more accessible in the 18PC membranes whose thickness is closest to that of dark-adapted thylakoid membranes [35,36]. A preference for specific membrane thicknesses has also been shown in other intrinsic membrane proteins [32,68-71]. It appears that when placed in either 10PC or 24PC membrane, LHCII is much more likely to reside in a quenched conformation than in 18PC, one tuned for light harvesting. Furthermore, the results on the Chl insertion ratio proved the best matching of LHCII protein with the 18 ACL. It is likely that changes in the orientation of Chls and carotenoids in LHCII, induced here by changes in membrane thickness, direct LHCII into a quenched state. It is interesting that LHCII appears to intrinsically default to a quenched state when the membrane environment is altered. Indeed, due to the high concentration of pigments within the complex [45], it appears harder to retain the light-harvesting state rather than a quenched one.

Interestingly, whilst the 10PC and 24PC display similar average fluorescence lifetimes, the 77K fluorescence emission spectra are highly divergent. Thus, despite similar amounts of quenching, here LHCII is represented in two separate quenched conformations. The 24PC condition displays a spectrum highly similar to environments, in which LHCII is aggregated, as shown by the prominent F700 [34,52,72]. However, the 10PC condition displays a large broadened 685 nm band, which appears to resemble the spectra of LHCII immobilized in gels [22], probably reflecting a particular quenched conformation of LHCII.

4.3 Hydrophobic mismatch as the driving force of qE?

Previously, it has been shown that both thinning of the lipid membrane or the flattening of proteins within can control both dynamics and conformations of each on both individual and ensemble levels [29,33,51,73]. Through a process known as hydrophobic mismatch, changes between the vertical hydrophobic lengths of the protein or lipid fractions of the membrane can control the orientation of the protein in the membrane [27,74,75], its accessible conformations [32], and its aggregation state in the membrane [76,77]. The structure of the solvent has been shown to be highly important in controlling the conformations of LHCII in detergent [78]. Thus, any changes in the lipid structure around LHCII will likely greatly affect its function *in vivo* [14,54,79]. It is well accepted that the thylakoid membrane becomes thinner upon illumination [15,16,80], however, it was only shown relatively recently that this tendency correlates with the extent of qE, but neither the intensity of illumination nor magnitude of ΔpH [12].

In this work, we have constructed *in vitro* LHCII-containing proteoliposomes with a range of acyl chain lengths of lipid. Static control of the bilayer membrane thicknesses allows for accurately capturing the state of illumination-trigger membrane thinning *in vivo* [12,15,80] and its effects on NPQ in LHCII. We have shown that thinning of the hydrophobic lipid fraction of the membrane is able to drive LHCII into individual quenched conformations and likely into aggregated states as well. Although the phospholipid bilayer enables us to establish an *in vitro* system to mimic both the mismatch scenarios, the native thylakoid lipids do impart an important influence on proteins. The lipid composition in thylakoid membrane is a mixture of MGDG, DGDG, SQDG and PG [60,81,82], and more than 90% of lipids reside in the bilayer locus [83]. Some of the MGDG and PG are integrated into the LHCII complex itself, and are responsible for LHCII trimerization and energy transfer efficiency [45,83,84]. Due to the conical shape of MGDG matching the hourglass shape of the LHCII, it provides lateral pressure in stabilizing trimeric LHCII [79]. Moreover, molecular dynamics simulations confirmed that the presence of MGDG leads to a significant increase of the physical pressure in the hydrophobic fatty acid moiety [85]. Changes in the lateral pressure profile may cause the neoxanthin distortion and the LHCII conformational change seen in the NPQ state [54]. Furthermore, the situation *in vivo* may be more complicated. Molecular

dynamics simulations have indicated that at low pH LHCII undergoes a conformational change into a quenched conformation where PsbS has been proposed to block the thylakoid lipid DGDG rearrangement, and allow LHCII transition into the quenched state, thus acting as a seeding point for further aggregation [12-14]. Thus, the nature of PsbS action within the hydrophobic mismatch state of LHCII remains to be further investigated, *in vivo* [5,7,12,86-88]. Furthermore, we would like to note that whilst the 10PC and 24PC conditions cause a quenching of LHCII from ~2 ns to ~500 ps, the quenching of 14PC is smaller (~1.5 ns). This is particularly interesting as the 18PC to 14PC transition appears to most closely reflect the *in vivo* thinning of the thylakoid membrane of ~20% [80], which would only cause 25% decrease in the lifetime. Thus, it may be the case that specifically membrane thinning alone is not adequate to trigger qE *in vivo*. The effect of membrane thinning alongside the effects of ΔpH and the allosteric modulation of zeaxanthin and PsbS upon the qE locus, LHCII, remain fruitful topics for further exploration, as emphasized in other works on LHCII in proteoliposomes [60,89-91]. However, it may be the case that unlike the scenario laid out above (i.e. positive mismatch), the LHCII protein becomes thinner relative to the membrane (i.e. negative mismatch). Molecular dynamics simulations and linear dichroism spectra appear to show that LHCII becomes effectively flatter when in the quenched state [26,92]. The observed membrane thinning in the light may thus be caused by a flattening of LHCII rather than a change in the lipid phase of the membrane [12,15,16,80]. Under this scenario, comparing 24PC to 18PC may be an attractive scenario. Between these conditions, there is a large amount of quenching despite only a 25% change in the ACL. Therefore, the effects of PsbS, ΔpH, and zeaxanthin may allow this previously observed flattening of LHCII, giving the energetic drive for LHCII aggregation through negative rather than positive mismatch.

In conclusion, we have shown that membrane thinning can induce quenching in LHCII. To disentangle the effects of protein-protein and protein-lipid interactions on the LHCII photoprotective switch, we have compared the structural and biophysical properties of LHCII proteoliposomes with varying ACL. Whilst the highest light-harvesting efficiency of LHCII is in a membrane of 18 carbons in ACL, similar to the *in vivo* thylakoid, further shortening or lengthening of the ACL will effectively quench LHCII and may provide the drive for LHCII aggregation. We further successfully separated two divergently quenched conformations of LHCII in 10PC proteoliposome. We suggest that hydrophobic mismatching between the vertical hydrophobic lengths of LHCII and lipids in the membrane could be the main driving force for qE *in vivo*. In essence, the hydrophobic mismatch between LHCII and surrounding proteins and lipids provides the energetic drive to change LHCII from a light-harvesting to a photoprotective state. We believe the proteoliposomal proof-of-concept of the hydrophobic mismatch hypothesis adds another important dimension to further understanding the regulation of light harvesting in the thylakoid membrane.

Supplementary Information

Additional microscopic images and fluorescence lifetime fitting parameters.

Acknowledgments

We would like to thank Dr. Vasco Giovagnetti and Dr. Francesco Saccon for useful discussions on the work.

Author contributions

AVR designed the project; DL and SW performed the experiments; GM and DL carried out the microscopic experiments; DL wrote the first manuscript draft; DL and SW analyzed the data; all authors revised and approved the final manuscript.

Conflict of interest

The authors declare no conflict of interest.

Funding statement

This work has been supported by a China Scholarship Council PhD studentship (202006360048) and a Leverhulme Trust Grant (RPG-2020-144)

Data availability

All the data can be made available upon request.

References

[1] S.B. Powles, Photoinhibition of photosynthesis induced by visible light, Annu. Rev. Plant Physiol. 35 (1984) 15–44. https://doi.org/10.1146/annurev.pp.35.060184.000311.

[2] A.V. Ruban, R.G. Walters, P. Horton, The molecular mechanism of the control of excitation energy dissipation in chloroplast membranes. Inhibition of ⊿pH-dependent quenching of chlorophyll fluorescence by dicyclohexylcarbodiimide, FEBS Lett. 309 (1992) 175–179. https://doi.org/10.1016/0014-5793(92)81089-5.

[3] A.V. Ruban, M.P. Johnson, C.D.P. Duffy, The photoprotective molecular switch in the photosystem II antenna, Biochim. Biophys. Acta - Bioenerg. 1817 (2012) 167–181. https://doi.org/10.1016/j.bbabio.2011.04.007.

[4] A.V. Ruban, Nonphotochemical chlorophyll fluorescence quenching: Mechanism and effectiveness in protecting plants from photodamage, Plant Physiol. 170 (2016) 1903–1916. https://doi.org/10.1104/pp.15.01935.

[5] F. Saccon, V. Giovagnetti, M.K. Shukla, A.V. Ruban, Rapid regulation of photosynthetic light harvesting in the absence of minor antenna and reaction centre complexes, J. Exp. Bot. 71 (2020) 3626–3637. https://doi.org/10.1093/jxb/eraa126.

[6] M.P. Johnson, A.V. Ruban, Restoration of rapidly reversible photoprotective energy dissipation in the absence of PsbS protein by enhanced ΔpH, J. Biol. Chem. 286 (2011) 19973–19981. https://doi.org/10.1074/jbc.M111.237255.

[7] X.P. Li, A.M. Gilmore, S. Caffarri, R. Bassi, T. Golan, D. Kramer, K.K. Niyogi, Regulation of photosynthetic light harvesting involves intrathylakoid lumen pH sensing by the PsbS protein, J. Biol. Chem. 279 (2004) 22866–22874. https://doi.org/10.1074/jbc.M402461200.

[8] N. Liguori, S.R.R. Campos, A.M. Baptista, R. Croce, Molecular anatomy of plant photoprotective switches: The sensitivity of PsbS to the environment, residue by residue, J. Phys. Chem. Lett. 10 (2019) 1737–1742. https://doi.org/10.1021/acs.jpclett.9b00437.

[9] P. Horton, A.V. Ruban, D. Rees, A.A. Pascal, G. Noctor, A.J. Young, Control of the light-harvesting function of chloroplast membranes by aggregation of the LHCII chlorophyll-protein complex, FEBS Lett. 292 (1991) 1–4. https://doi.org/10.1016/0014-5793(91)80819-O.

[10] N. Betterle, M. Ballottari, S. Zorzan, S. de Bianchi, S. Cazzaniga, L. Dall'Osto, T. Morosinotto, R. Bassi, Light-induced dissociation of an antenna hetero-oligomer is needed for non-photochemical quenching induction, J. Biol. Chem. 284 (2009) 15255–15266. https://doi.org/10.1074/jbc.M808625200.

[11] M.P. Johnson, T.K. Goral, C.D.P. Duffy, A.P.R. Brain, C.W. Mullineaux, A.V. Ruban, Photoprotective energy dissipation involves the reorganization of photosystem II light-harvesting complexes in the grana membranes of spinach chloroplasts, Plant Cell. 23 (2011) 1468–1479.

https://doi.org/10.1105/tpc.110.081646.

[12] M.P. Johnson, A.P.R. Brain, A.V. Ruban, Changes in thylakoid membrane thickness associated with the reorganization of photosystem II light harvesting complexes during photoprotective energy dissipation, Plant Signal. Behav. 6 (2011) 1386–1390. https://doi.org/10.4161/psb.6.9.16503.

[13] T.K. Goral, M.P. Johnson, C.D.P. Duffy, A.P.R. Brain, A.V. Ruban, C.W. Mullineaux, Light-harvesting antenna composition controls the macrostructure and dynamics of thylakoid membranes in *Arabidopsis*, Plant J. 69 (2012) 289–301. https://doi.org/10.1111/j.1365-313X.2011.04790.x.

[14] V. Daskalakis, S. Papadatos, U. Kleinekathöfer, Fine tuning of the photosystem II major antenna mobility within the thylakoid membrane of higher plants, Biochim. Biophys. Acta - Biomembr. 1861 (2019) 183059. https://doi.org/10.1016/j.bbamem.2019.183059.

[15] S. Murakami, L. Packer, Light-induced changes in the conformation and configuration of the thylakoid membrane of *Ulva* and *Porphyra* chloroplasts *in vivo*, Plant Physiol. 45 (1970) 289–299. https://doi.org/10.1104/pp.45.3.289.

[16] S. Murakami, L. Packer, Protonation and chloroplast membrane structure, J. Cell Biol. 47 (1970) 332–51. http://www.ncbi.nlm.nih.gov/pubmed/19866735.

[17] A.V. Ruban, F. Calkoen, S.L.S. Kwa, R. Van Grondelle, P. Horton, J.P. Dekker, Characterisation of LHC II in the aggregated state by linear and circular dichroism spectroscopy, Biochim. Biophys. Acta - Bioenerg. 1321 (1997) 61–70. https://doi.org/10.1016/S0005-2728(97)00047-9.

[18] A.V. Ruban, P. Horton, B. Robert, Resonance raman spectroscopy of the photosystem II light-harvesting complex of green plants: A comparison of trimeric and aggregated states, Biochemistry. 34 (1995) 2333–2337. https://doi.org/10.1021/bi00007a029.

[19] A.V. Ruban, R. Berera, C. Ilioaia, I.H.M. Van Stokkum, J.T.M. Kennis, A.A. Pascal, H. Van Amerongen, B. Robert, P. Horton, R. Van Grondelle, Identification of a mechanism of photoprotective energy dissipation in higher plants, Nature. 450 (2007) 575–578. https://doi.org/10.1038/nature06262.

[20] M.P. Johnson, A.V. Ruban, Photoprotective energy dissipation in higher plants involves alteration of the excited state energy of the emitting chlorophyll(s) in the light harvesting antenna II (LHCII), J. Biol. Chem. 284 (2009) 23592–23601. https://doi.org/10.1074/jbc.M109.013557.

[21] B. Van Oort, A. Van Hoek, A.V. Ruban, H. Van Amerongen, Equilibrium between quenched and nonquenched conformations of the major plant light-harvesting complex studied with high-pressure time-resolved fluorescence, J. Phys. Chem. B. 111 (2007) 7631–7637. https://doi.org/10.1021/jp070573z.

[22] C. Ilioaia, M.P. Johnson, P. Horton, A.V. Ruban, Induction of efficient energy dissipation in the isolated light-harvesting complex of photosystem II in the absence of protein aggregation, J. Biol.

Chem. 283 (2008) 29505–29512. https://doi.org/10.1074/jbc.M802438200.

[23] G.S. Schlau-Cohen, H.Y. Yang, T.P.J. Krüger, P. Xu, M. Gwizdala, R. Van Grondelle, R. Croce, W.E. Moerner, Single-molecule identification of quenched and unquenched states of LHCII, J. Phys. Chem. Lett. 6 (2015) 860–867. https://doi.org/10.1021/ACS.JPCLETT.5B00034/SUPPL_FILE/JZ5B00034_SI_001.PDF.

[24] A. V Ruban, S. Wilson, The mechanism of non-photochemical quenching in plants: Localization and driving forces, Plant Cell Physiol. 62 (2020) 1063–1072. https://doi.org/10.1093/pcp/pcaa155.

[25] J.A. Killian, Hydrophobic mismatch between proteins and lipids in membranes, Biochim. Biophys. Acta - Biomembr. 1376 (1998) 401–416. https://doi.org/10.1016/S0304-4157(98)00017-3.

[26] H. Li, Y. Wang, M. Ye, S. Li, D. Li, H. Ren, M. Wang, L. Du, H. Li, G. Veglia, J. Gao, Y. Weng, Dynamical and allosteric regulation of photoprotection in light harvesting complex II, Sci. China Chem. 63 (2020) 1121–1133. https://doi.org/10.1007/s11426-020-9771-2.

[27] J. Lee, W. Im, Restraint potential and free energy decomposition formalism for helical tilting, Chem. Phys. Lett. 441 (2007) 132–135. https://doi.org/10.1016/j.cplett.2007.05.003.

[28] Y. Tahara, Y. Fujiyoshi, A new method to measure bilayer thickness: Cryo-electron microscopy of frozen hydrated liposomes and image simulation, Micron. 25 (1994) 141–149. https://doi.org/10.1016/0968-4328(94)90029-6.

[29] D. Milovanovic, A. Honigmann, S. Koike, F. Göttfert, G. Pähler, M. Junius, S. Müllar, U. DIederichsen, A. Janshoff, H. Grubmüller, H.J. Risselada, C. Eggeling, S.W. Hell, G. Van Den Bogaart, R. Jahn, Hydrophobic mismatch sorts SNARE proteins into distinct membrane domains, Nat. Commun. 6 (2015) 1–10. https://doi.org/10.1038/ncomms6984.

[30] W. Dowhan, Molecular basis for membrane phospholipid diversity: Why are there so many lipids? Annu. Rev. Biochem. 66 (1997) 199–232. https://doi.org/10.1146/annurev.biochem.66.1.199.

[31] T. Gil, J.H. Ipsen, O.G. Mouritsen, M.C. Sabra, M.M. Sperotto, M.J. Zuckermann, Theoretical analysis of protein organization in lipid membranes, Biochim. Biophys. Acta - Biomembr. 1376 (1998) 245–266. https://doi.org/10.1016/S0304-4157(98)00022-7.

[32] F. Dumas, M.C. Lebrun, J.F. Tocanne, Is the protein/lipid hydrophobic matching principle relevant to membrane organization and functions? FEBS Lett. 458 (1999) 271–277. https://doi.org/10.1016/S0014-5793(99)01148-5.

[33] T. Kim, W. Im, Revisiting hydrophobic mismatch with free energy simulation studies of transmembrane helix tilt and rotation, Biophys. J. 99 (2010) 175–183. https://doi.org/10.1016/j.bpj.2010.04.015.

[34] S. Wilson, D.-H. Li, A.V Ruban, The structural and spectral features of light-harvesting complex II proteoliposomes mimic those of native thylakoid membranes, J. Phys. Chem. Lett. 13 (2022) 5683−5691. https://doi.org/10.1021/acs.jpclett.2c01019.

[35] F. Zhou, S. Liu, Z. Hu, T. Kuang, H. Paulsen, C. Yang, Effect of monogalactosyldiacylglycerol on the interaction between photosystem II core complex and its antenna complexes in liposomes of thylakoid lipids, Photosynth. Res. 99 (2009) 185–193. https://doi.org/10.1007/s11120-008-9388-9.

[36] A.V. Ruban, The Photosynthetic Membrane, Wiley, United Kingdom, 2013. https://doi.org/10.1002/9781118447628.ch3.

[37] E. Belgio, M.P. Johnson, S. Jurić, A.V. Ruban, Higher plant photosystem II light-harvesting antenna, not the reaction center, determines the excited-state lifetime—Both the maximum and the nonphotochemically quenched, Biophys. J. 102 (2012) 2761–2771. https://doi.org/10.1016/j.bpj.2012.05.004.

[38] J. Chmeliov, A. Gelzinis, E. Songaila, R. Augulis, C.D.P. Duffy, A.V. Ruban, L. Valkunas, The nature of self-regulation in photosynthetic light-harvesting antenna, Nat. Plants. 2 (2016) 1–7. https://doi.org/10.1038/NPLANTS.2016.45.

[39] A.V. Ruban, A.J. Young, A.A. Pascal, P. Horton, The effects of illumination on the xanthophyll composition of the photosystem II light-harvesting complexes of spinach thylakoid membranes, Plant Physiol. 104 (1994) 227–234. https://doi.org/10.1104/pp.104.1.227.

[40] M.K. Shukla, A. Watanabe, S. Wilson, V. Giovagnetti, E.I. Moustafa, J. Minagawa, A.V. Ruban, A novel method produces native light-harvesting complex II aggregates from the photosynthetic membrane revealing their role in nonphotochemical quenching, J. Biol. Chem. 295 (2020) 17816–17826. https://doi.org/10.1074/jbc.RA120.016181.

[41] A.V. Ruban, P. Horton, The xanthophyll cycle modulates the kinetics of nonphotochemical energy dissipation in isolated light-harvesting complexes, intact chloroplasts, and leaves of spinach, Plant Physiol. 119 (1999) 531–542. https://doi.org/10.1104/pp.119.2.531.

[42] R.J. Porra, W.A. Thompson, P.E. Kriedemann, Determination of accurate extinction coefficients and simultaneous equations for assaying chlorophylls *a* and *b* extracted with four different solvents: verification of the concentration of chlorophyll standards by atomic absorption spectroscopy, Biochim. Biophys. Acta. 975 (1989) 384–394.

[43] M.N. Jones, Use of liposomes to deliver bactericides to bacterial biofilms, Methods Enzymol. 391 (2005) 211–228. https://doi.org/10.1016/S0076-6879(05)91013-6.

[44] S.C. Costigan, P.J. Booth, R.H. Templer, Estimations of lipid bilayer geometry in fluid lamellar phases, Biochim. Biophys. Acta - Biomembr. 1468 (2000) 41–54. https://doi.org/10.1016/S0005-2736(00)00220-0.

[45] Z. Liu, H. Yan, K. Wang, T. Kuang, J. Zhang, L. Gui, X. An, W. Chang, Crystal structure of spinach major light-harvesting complex at 2.72 Å resolution, Nature. 428 (2004) 287–292. https://doi.org/10.1038/nature02373.

[46] W.R. Bowen, A. Mongruel, Calculation of the collective diffusion coefficient of electrostatically

stabilised colloidal particles, Colloids Surfaces A Physicochem. Eng. Asp. 138 (1998) 161–172. https://doi.org/10.1016/S0927-7757(96)03954-4.

[47] D.N. Mastronarde, Automated electron microscope tomography using robust prediction of specimen movements, J. Struct. Biol. 152 (2005) 36–51. https://doi.org/10.1016/j.jsb.2005.07.007.

[48] C.A. Schneider, W.S. Rasband, K.W. Eliceiri, NIH image to imageJ: 25 years of image analysis, Nat. Methods. 9 (2012) 671–675. https://doi.org/10.1038/nmeth.2089.

[49] E. Fišerová, M. Kubala, Mean fluorescence lifetime and its error, J. Lumin. 132 (2012) 2059–2064. https://doi.org/10.1016/j.jlumin.2012.03.038.

[50] R. Douce, J. Joyard, in: D.R. Ort, C.F. Yocum (Eds.) Biosynthesis of thylakoid membrane lipids, Oxyg. Photosynth. Light React. 1996, 69–101.

[51] K. Mitra, I. Ubarretxena-Belandia, T. Taguchi, G. Warren, D.M. Engelman, Modulation of the bilayer thickness of exocytic pathway membranes by membrane proteins rather than cholesterol, Proc. Natl. Acad. Sci. U. S. A. 101 (2004) 4083–4088. https://doi.org/10.1073/pnas.0307332101.

[52] A. Natali, J.M. Gruber, L. Dietzel, M.C.A. Stuart, R. Van Grondelle, R. Croce, Light-harvesting complexes (LHCs) cluster spontaneously in membrane environment leading to shortening of their excited state lifetimes, J. Biol. Chem. 291 (2016) 16730–16739. https://doi.org/10.1074/jbc.M116.730101

[53] I. Simidjiev, S. Stoylova, H. Amenitsch, T. Jávorfi, L. Mustárdy, P. Laggner, A. Holzenburg, G. Garab, Self-assembly of large, ordered lamellae from non-bilayer lipids and integral membrane proteins *in vitro*, Proc. Natl. Acad. Sci. U. S. A. 97 (2000) 1473–1476. https://doi.org/10.1073/pnas.97.4.1473.

[54] S. Tietz, M. Leuenberger, P. Horner, A.H. Olson, G.R. Fleming, H. Kirchhoff, A proteoliposome-based system reveals how lipids control photosynthetic light harvesting, J. Biol. Chem. 295 (2020) 1857–1866. https://doi.org/10.1074/jbc.RA119.011707.

[55] J. Lemmich, K. Mortensen, J.H. Ipsen, T. Hønger, R. Bauer, O.G. Mouritsen, Small-angle neutron scattering from multilamellar lipid bilayers: Theory, model, and experiment, Phys. Rev. E. 53 (1996) 5169–5180. https://doi.org/10.1103/PhysRevE.53.5169.

[56] B.A. Lewis, D.M. Engelman, Lipid bilayer thickness varies linearly with acyl chain length in fluid phosphatidylcholine vesicles, J. Mol. Biol. 166 (1983) 211–217. https://doi.org/10.1016/S0022-2836(83)80007-2.

[57] R.N. Lewis, N.M. Nanette Mak, R.N. McElhaney, A differential scanning calorimetric study of the thermotropic phase behavior of model membranes composed of phosphatidylcholines containing linear saturated fatty acyl chains, Biochemistry. 26 (1987) 6118–6126. https://doi.org/10.1021/bi00393a026.

[58] J. Peschke, J. Riegler, H. Möhwald, Quantitative analysis of membrane distortions induced by mismatch of protein and lipid hydrophobic thickness, Eur. Biophys. J. 14 (1987) 385–391.

https://doi.org/10.1007/BF00254861.

[59] B. Piknová, E. Pérochon, J.-F. Tocanne, Hydrophobic mismatch and long-range protein/lipid interactions in bacteriorhodopsidphosphatidylcholine vesicles, Eur. J. Biochem. 218 (1993) 385–396.

[60] L. Wilk, M. Grunwald, P.N. Liao, P.J. Walla, W. Kühlbrandt, Direct interaction of the major light-harvesting complex II and PsbS in nonphotochemical quenching, Proc. Natl. Acad. Sci. U. S. A. 110 (2013) 5452–5456. https://doi.org/10.1073/pnas.1205561110.

[61] M. Tutkus, P. Akhtar, J. Chmeliov, F. Görföl, G. Trinkunas, P.H. Lambrev, L. Valkunas, Fluorescence microscopy of single liposomes with incorporated pigment-proteins, Langmuir. 34 (2018) 14410–14418. https://doi.org/10.1021/acs.langmuir.8b02307.

[62] A. Pandit, N. Shirzad-Wasei, L.M. Wlodarczyk, H. Van Roon, E.J. Boekema, J.P. Dekker, W.J. De Grip, Assembly of the major light-harvesting complex II in lipid nanodiscs, Biophys. J. 101 (2011) 2507–2515. https://doi.org/10.1016/j.bpj.2011.09.053.

[63] E. Crisafi, A. Pandit, Disentangling protein and lipid interactions that control a molecular switch in photosynthetic light harvesting, Biochim. Biophys. Acta - Biomembr. 1859 (2017) 40–47. https://doi.org/10.1016/j.bbamem.2016.10.010.

[64] M. Son, A. Pinnola, S.C. Gordon, R. Bassi, G.S. Schlau-Cohen, Observation of dissipative chlorophyll-to-carotenoid energy transfer in light-harvesting complex II in membrane nanodiscs, Nat. Commun. 11 (2020) 1–8. https://doi.org/10.1038/s41467-020-15074-6.

[65] A.M. Hancock, M. Son, M. Nairat, D. Wei, L.J.C. Jeuken, C.D.P. Duffy, G.S. Schlau-Cohen, P.G. Adams, Ultrafast energy transfer between lipid-linked chromophores and plant light-harvesting complex II, Phys. Chem. Chem. Phys. 23 (2021) 19511–19524. https://doi.org/10.1039/d1cp01628h.

[66] M. Son, R. Moya, A. Pinnola, R. Bassi, G.S. Schlau-Cohen, Protein-protein interactions induce pH-dependent and zeaxanthin-independent photoprotection in the plant light-harvesting complex, LHCII, J. Am. Chem. Soc. 143 (2021) 17577–17586. https://doi.org/10.1021/jacs.1c07385.

[67] P. Akhtar, F. Görföl, G. Garab, P.H. Lambrev, Dependence of chlorophyll fluorescence quenching on the lipid-to-protein ratio in reconstituted light-harvesting complex II membranes containing lipid labels, Chem. Phys. 522 (2019) 242–248. https://doi.org/10.1016/j.chemphys.2019.03.012.

[68] A. Johannsson, C.A. Keightley, G.A. Smith, C.D. Richards, T.R. Hesketh, J.C. Metcalfe, The effect of bilayer thickness and *n*-alkanes on the activity of the (Ca^{2+} + Mg^{2+})-dependent ATPase of Sarcoplasmic reticulum, J. Biol. Chem. 256 (1981) 1643–1650. https://doi.org/10.1016/S0021-9258(19)69855-8.

[69] A.P. Starling, J.M. East, A.G. Lee, Effects of phosphatidylcholine fatty acyl chain length on calcium binding and other functions of the (Ca^{2+}–Mg^{2+})-ATPase, Biochemistry. 32 (1993) 1593–1600. https://doi.org/10.1021/bi00057a025.

[70] R.L. Cornea, D.D. Thomas, Effects of membrane thickness on the molecular dynamics and enzymatic activity of reconstituted Ca-ATPase, Biochemistry. 33 (1994) 2912–2920. https://doi.org/10.1021/bi00176a022.

[71] S.J. Slater, M.B. Kelly, F.J. Taddeo, C. Ho, E. Rubin, C.D. Stubbs, The modulation of protein kinase C activity by membrane lipid bilayer structure., J. Biol. Chem. 269 (1994) 4866–4871. https://doi.org/10.1016/S0021-9258(17)37624-X.

[72] A.V. Ruban, D. Rees, A.A. Pascal, P. Horton, Mechanism of ⊿pH-dependent dissipation of absorbed excitation energy by photosynthetic membranes. II. The relationship between LHCII aggregation in vitro and qE in isolated thylakoids, Biochim. Biophys. Acta - Bioenerg. 1102 (1992) 39–44. https://doi.org/10.1016/0005-2728(92)90062-7.

[73] E. Navakoudis, T. Stergiannakos, V. Daskalakis, A perspective on the major light-harvesting complex dynamics under the effect of pH, salts, and the photoprotective PsbS protein, Photosynth. Res. (2022). https://doi.org/10.1007/s11120-022-00935-6.

[74] J. Lee, W. Im, Transmembrane helix tilting: Insights from calculating the potential of mean force, Phys. Rev. Lett. 100 (2008) 1–4. https://doi.org/10.1103/PhysRevLett.100.018103.

[75] Y. Gofman, T. Haliloglu, N. Ben-Tal, The transmembrane helix tilt may be determined by the balance between precession entropy and lipid perturbation, J. Chem. Theory Comput. 8 (2012) 2896–2904. https://doi.org/10.1021/ct300128x.

[76] C. Nielsen, M. Goulian, O.S. Andersen, Energetics of inclusion-induced bilayer deformations, Biophys. J. 74 (1998) 1966–1983. https://doi.org/10.1016/S0006-3495(98)77904-4.

[77] N. Dan, S.A. Safran, Effect of lipid characteristics on the structure of transmembrane proteins, Biophys. J. 75 (1998) 1410–1414. https://doi.org/10.1016/S0006-3495(98)74059-7.

[78] F. Li, C. Liu, S. Streckaite, C. Yang, P. Xu, M.J. Llansola-Portoles, C. Ilioaia, A.A. Pascal, R. Croce, B. Robert, A new, unquenched intermediate of LHCII, J. Biol. Chem. (2021) 100322. https://doi.org/10.1016/j.jbc.2021.100322.

[79] D. Seiwert, H. Witt, A. Janshoff, H. Paulsen, The non-bilayer lipid MGDG stabilizes the major light-harvesting complex (LHCII) against unfolding, Sci. Rep. 5 (2017) 5158. https://doi.org/10.1038/s41598-017-05328-7.

[80] H. Kirchhoff, C. Hall, M. Wood, M. Herbstová, O. Tsabari, R. Nevo, D. Charuvi, E. Shimoni, Z. Reich, Dynamic control of protein diffusion within the granal thylakoid lumen, Proc. Natl. Acad. Sci. U. S. A. 108 (2011) 20248–20253. https://doi.org/10.1073/pnas.1104141109.

[81] K. Kobayashi, K. Endo, H. Wada, Specific distribution of phosphatidylglycerol to photosystem complexes in the thylakoid membrane, Front. Plant Sci. 8 (2017) 1–7. https://doi.org/10.3389/fpls.2017.01991.

[82] C. Yang, S. Boggasch, W. Haase, H. Paulsen, Thermal stability of trimeric light-harvesting chlorophyll a/b complex (LHCIIb) in liposomes of thylakoid lipids, Biochim. Biophys. Acta -

Bioenerg. 1757 (2006) 1642–1648. https://doi.org/10.1016/j.bbabio.2006.08.010.

[83] A. Yoshihara, K. Kobayashi, Lipids in photosynthetic protein complexes in the thylakoid membrane of plants, algae, and cyanobacteria, J. Exp. Bot. (2022). https://doi.org/10.1093/jxb/erac017.

[84] X. Pan, Z. Liu, M. Li, W. Chang, Architecture and function of plant light-harvesting complexes II, Curr. Opin. Struct. Biol. 23 (2013) 515–525. https://doi.org/10.1016/j.sbi.2013.04.004.

[85] K. Baczynski, M. Markiewicz, M. Pasenkiewicz-Gierula, A computer model of a polyunsaturated monogalactolipid bilayer, Biochimie. 118 (2015) 129–140. https://doi.org/10.1016/j.biochi.2015.09.007.

[86] V. Correa-Galvis, G. Poschmann, M. Melzer, K. Stühler, P. Jahns, PsbS interactions involved in the activation of energy dissipation in Arabidopsis, Nat. Plants. 2 (2016) 1–8. https://doi.org/10.1038/NPLANTS.2015.225.

[87] M. Krishnan-Schmieden, P. Konold, J. Kennis, A. Pandit, The molecular pH-response mechanism of the plant light-stress sensor PsbS, Nat. Commun. 12 (2021) 1-11. https://doi.org/10.1101/457614.

[88] R. Welc, R. Luchowski, D. Kluczyk, M. Zubik-Duda, W. Grudzinski, M. Maksim, E. Reszczynska, K. Sowinski, R. Mazur, A. Nosalewicz, W.I. Gruszecki, Mechanisms shaping the synergism of zeaxanthin and PsbS in photoprotective energy dissipation in the photosynthetic apparatus of plants, Plant J. 107 (2021) 418–433. https://doi.org/10.1111/tpj.15297.

[89] C. Liu, Z. Gao, K. Liu, R. Sun, C. Cai, A.R. Holzwarth, C. Yang, Simultaneous refolding of denatured PsbS and reconstitution with LHCII into liposomes of thylakoid lipids, Photosynth. Res. 127 (2016) 109–116. https://doi.org/10.1007/s11120-015-0176-z.

[90] K. Pawlak, S. Paul, C. Liu, M. Reus, C. Yang, A.R. Holzwarth, On the PsbS-induced quenching in the plant major light-harvesting complex LHCII studied in proteoliposomes, Photosynth. Res. 144 (2020) 195–208. https://doi.org/10.1007/s11120-020-00740-z.

[91] L. Nicol, R. Croce, The PsbS protein and low pH are necessary and sufficient to induce quenching in the light-harvesting complex of plants LHCII, Sci. Rep. 11 (2021) 1–8. https://doi.org/10.1038/s41598-021-86975-9.

[92] M. Wentworth, A.V. Ruban, P. Horton, Thermodynamic investigation into the mechanism of the chlorophyll fluorescence quenching in isolated photosystem II light-harvesting complexes, J. Biol. Chem. 278 (2003) 21845–21850. https://doi.org/10.1074/jbc.m302586200.

Declaration of interests

☐The authors declare that they have no known competing financial interests or personal relationships that could have appeared to influence the work reported in this paper.

☒The authors declare the following financial interests/personal relationships which may be considered as potential competing interests:

Alexander V. Ruban reports financial support was provided by Queen Mary University of London.

Altered lipid acyl chain length controls energy dissipation in light-harvesting complex II proteoliposomes by hydrophobic mismatch

Dan-Hong Li[a], Sam Wilson[a], Giulia Mastroianni[a], Alexander V. Ruban[a*]

[a] Department of Biochemistry, School of Biological and Behavioural Sciences, Queen Mary University of London, London, E1 4NS, United Kingdom

Conflict of interest

The authors declare no conflict of interest.

Highlight *(three to five bullet points, no more than 85 characters)*

- Reconstitution of LHCII protein into liposomes with altered fatty acid chain length
- Two quenched conformations of LHCII are physically separated
- Hydrophobic mismatch is a probable trigger of the quenching, qE
- Membrane thickness balances energy between light-harvesting and dissipative states